Chirality transfer induced spin selectivity effect in a molecule-metal heterojunction

Mengzhao Du,* Xuan Liu,* Xiaohui Liu,† and Shijie Xie‡
School of Physics, State Key Laboratory of Crystal Materials, Shandong University, Ji'nan 250100, China

(Received 8 February 2023; revised 29 June 2023; accepted 29 August 2023; published 14 September 2023)

The chiral geometry of the organic molecule is considered to be crucial to the chiral-induced spin selectivity (CISS) effect. However, the fundamental mechanism responsible for CISS is still debated. In this paper, we propose a mechanism of chirality transfer from chiral molecules to metals by interface coupling in a molecule/metal heterojunction. It is found that the transferred charges present a chiral distribution even in the achiral metal. Using a tight-binding model and tunneling theory, we focus on the induced chiral interface and the strong spin-orbit coupling of the metal, and predict a sizable CISS effect. This work provides a different perspective for us to understand the CISS effect.

DOI: 10.1103/PhysRevB.108.125419

I. INTRODUCTION

Chiral-induced spin selectivity (CISS) effect, which was observed in systems with broken symmetry of chirality, results from the coupling of the moving spin and chirality due to the spin-orbit coupling (SOC) [1–5]. In a chiral system, the spin asymmetry of the transport electrons depends on its chirality. For example, the introduction of chiral molecules leads to chirality-dependent photoelectric effect and electric transport effect [6–9]. Promisingly, the CISS effect makes it possible to control the spin degree of freedom of electrons without an external magnetic field, thus allowing the use of electron spin to process information in memory and logic devices without the need for a permanent magnetized ferromagnet [10–12], as well as the construction of chiral-induced spin light-emitting diode devices [13] and efficient chiral-molecule-based switching of magnetic systems at room temperature [14,15]. Even though the great potential of applications of the CISS effect on spintronics is promising and the development in this field is fast, the fundamental mechanism of it is still debated. Guo *et al.* suggested that the moving electrons are subjected to a helical electrostatic potential in a chiral molecule, resulting in the so-called chiral-induced SOC which is responsible for the spin-polarized transmission [16,17]. In experiments, the chirality is usually introduced by chiral organic molecules. Considering the strong electron-phonon coupling of organic materials, the resulting polaron transport within a helical molecule is also important for spin polarization, and a synergistic effect of the carrier velocity and density on CISS is proposed [18,19]. Fransson studied the effects of SOC interactions on spin-dependent electron-phonon coupling and found that it results in exchange splitting between spin channels and leads to a spin polarization of tens of percent [20] which could even be enhanced by taking into account the electron correlation [21]. We need to note that, for chiral organic molecules, obviously large parameters for chiral-induced SOC are usually inevitable to get considerable CISS to make the theoretical results comparable with the experimental findings. As we know, however, organic materials are composed of light elements with low atomic numbers where SOC is quite weak. In addition, the SOC from the geometry of chiral organic molecules should be of the order of a few millielectron volts, which is also too small to explain the experimentally detected strong spin polarization. Considering the real situation in CISS experiments where chiral molecules are deposited or adsorbed on metal substrates [22–24], Yan *et al.* proposed that the strong SOC of the metal substrate plays a crucial role to induce CISS. They indicated that the spin and orbit are locked within the metal due to the strong SOC of it, and the electrons with orbital angular momentum matching the molecular chirality are easier to cross the interface and enter the chiral layer. Therefore, an orbital selectivity, together with a spin selectivity, takes place at the interface [25]. By considering the strong SOC in the electrodes, Alwan *et al.* showed that the spin-transfer torque effect could cause substantial orbital angular momentum polarization to induce the spin polarization observed in experiments [26].

Besides the achievements in experiments and theory, the fundamental understanding of CISS and the related chirality-dependent phenomena is still not clear. Previous studies revealed that the CISS effect is complicated and not ascribed to a single parameter. Whether there are other unrevealed chiral factors that contribute to the CISS effect is not only of fundamental interest but has practical meaning for novel spintronic device design [27–31]. In this paper, we propose a different perspective to understand the CISS effect—the chirality transfer mechanism. When the metal substrate is in contact with chiral molecules, a chiral charge distribution will be induced in the metal, and a spin preference matching the chirality appears in the metal combined with strong SOC. We studied the effects of the induced chiral charge distribution on CISS by modeling the tunneling of electrons. Our theoretical

*These authors contributed equally to this work.
†Corresponding author: liuxiaohui@sdu.edu.cn
‡Corresponding author: xsj@sdu.edu.cn

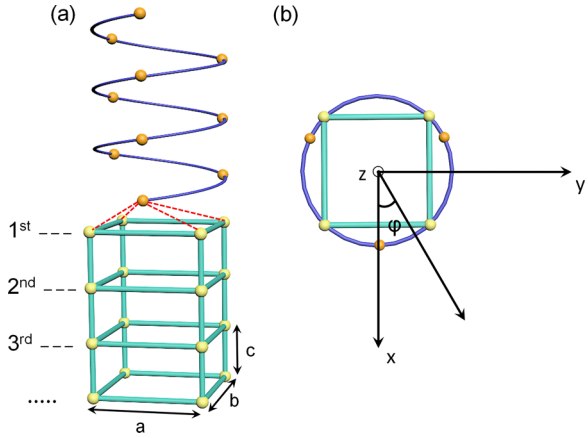

FIG. 1. Schematic of the side view (a) and the top view (b) of the modeled right-handed helix/metal heterojunction. The red dashed line in (a) indicates the long-range transition between the helical molecule and the metal layers.

results match well with the experimental studies and demonstrate the importance of chirality of charge density on CISS.

II. MODEL AND CALCULATIONS

At the interface of a molecule/metal heterojunction, charge redistribution takes place due to the chemical potential difference. To study its impact on CISS, we consider a system which is shown schematically in Fig. 1, where the metal layers are modeled by a simple orthogonal structure with lattice parameters $a = b = 2c = 0.4$ nm and the chiral molecule is modeled by a helical chain with the helix angle $\theta = 45^\circ$, the twist angle $\Delta\varphi = 120^\circ$, and the helix radius $R = \sqrt{2}c$. The fourfold rotational symmetry axis of the metal and the helical axis of the helical molecule coincide with the z axis, and the vertical height of the helical molecule from the metal surface is 0.2 nm.

The Hamiltonian of the system is depicted as

$$\hat{H} = \hat{H}_{\rm M} + \hat{H}_{\rm P} + \hat{H}_{\rm C}, \tag{1}$$

where $\hat{H}_{\rm M}$ and $\hat{H}_{\rm P}$ are the Hamiltonians of the metal and the helical chain, respectively. In the framework of the tight-binding approach, they are written as

$$\hat{H}_{\rm M} = \sum_n \varepsilon_{\rm M} c_n^\dagger c_n - \sum_{n\neq m} t_{n,m} c_n^\dagger c_m + \sum_{n\neq m} {\rm i}\alpha_{n,m} c_n^\dagger \left(\mathbf{e}_{n,m}^E \times \mathbf{e}_{n,m}^p\right)\cdot\hat{\boldsymbol{\sigma}} c_m + {\rm H.c.} \tag{2}$$

and

$$\hat{H}_{\rm P} = \sum_n \varepsilon_{\rm P} a_n^\dagger a_n - \sum_{n\neq m} \tau_{n,m} a_n^\dagger a_m + {\rm H.c.}, \tag{3}$$

where $c_n^\dagger = (c_{n\uparrow}^\dagger, c_{n\downarrow}^\dagger)$ and c_n are the creation and annihilation operators of two-component spinors at site n. $\varepsilon_{\rm M}$ and $\varepsilon_{\rm P}$ are the on-site energies of the metal and the molecule, respectively. $t_{n,m} = t_0 e^{-(|\mathbf{R}_m - \mathbf{R}_n| - l_{\rm M})/l_{\rm M}}$ is the transfer integral in the metal, and the transfer integral of the chiral molecule closely related to its helical configuration is written as $\tau_{n,m} = \tau_0 e^{-(|\mathbf{R}_m - \mathbf{R}_n| - l_{\rm P})/l_{\rm P}} = \tau_0 e^{-(\sqrt{4R^2\sin^2[(n-m)\Delta\varphi/2] + (n-m)^2(R\Delta\varphi\tan\theta)^2} - l_{\rm P})/l_{\rm P}}$, where $\mathbf{R}_n$ is the position vector of site n. In our model, the transfer integrals are long-ranged and decay exponentially, with $l_{\rm M} = c$ and $l_{\rm P} = 2\sqrt{3}c$ being the decay lengths of the metal and helical chain respectively. Since the SOC of the metal is much stronger than that of the organic molecule, to highlight its effect on CISS, we only include the SOC of the metal layers in the present model which is indicated by the third term in Eq. (2) where $\hat{\boldsymbol{\sigma}}$ is the Pauli vector operator. For an electron hopping from site n to m, $\mathbf{e}_{n,m}^p$ denotes the direction vector of the momentum pointing from $\mathbf{R}_n$ to $\mathbf{R}_m$ and $\mathbf{e}_{n,m}^E$ is the direction vector of the electric field at $\mathbf{R}_{n,m} = (\mathbf{R}_n + \mathbf{R}_m)/2$. We consider the SOC interaction $\alpha_{n,m} = \alpha_0 e^{-(|\mathbf{R}_m - \mathbf{R}_n| - l_{\rm M})/l_{\rm M}}$ to be long-ranged and decay exponentially with the same ratio of electron transfer. The Hamiltonian $\hat{H}_{\rm C}$ describes the coupling between the helical molecule and the metal layers. By considering the long-range coupling within the tight-binding approximation, the Hamiltonian is written as

$$\hat{H}_{\rm C} = -\sum_{n,m} \gamma_{n,m} a_n^\dagger c_m + {\rm H.c.}, \tag{4}$$

where the transfer integral is represented as $\gamma_{n,m} = \gamma_0 e^{-(|\mathbf{R}_m - \mathbf{R}_n| - l_{\rm C})/l_{\rm C}}$ with $l_{\rm C} = (l_{\rm M} + l_{\rm P})/2$. The static Schrödinger equation $\hat{H}\psi_\mu = \varepsilon_\mu \psi_\mu$ with the electronic eigenwave function $\psi_\mu = \sum_{n,s} Z_{\mu,n,s} |n, s\rangle$ and eigenvalue ε_μ could be solved. Then the charge distribution in the whole system, i.e., the charge at site n is given by $q_n = \sum_s q_{n,s} = \sum_{\mu,s} Z_{\mu,n,s}^* f_\mu Z_{\mu,n,s}$ with f_μ the Fermi occupation.

In our calculations, the following parameters are set: $\varepsilon_{\rm M} = 1.0$ eV, $\varepsilon_{\rm P} = 0$ eV, for transfer integrals: $t_0 = 1.8$ eV, $\tau_0 = 1.2$ eV, $\gamma_0 = 1.0$ eV, and for SOC strength $\alpha_0 = 0.15$ eV.

For the simplest case that one Au atom is coupled with one C atom, the charge distribution is given analytically by $q_{\rm Au} = \gamma^2/[\gamma^2 + (\varepsilon_{\rm M} - \varepsilon_-)^2]$ and $q_{\rm C} = (\varepsilon_{\rm M} - \varepsilon_-)^2/[\gamma^2 + (\varepsilon_{\rm M} - \varepsilon_-)^2]$ where $\varepsilon_- = [\varepsilon_{\rm M} + \varepsilon_{\rm P} - \sqrt{(\varepsilon_{\rm M} - \varepsilon_{\rm P})^2 + 4\gamma^2}]/2$ is the ground state energy and γ denotes the coupling between Au and C atoms. Obviously, we could see that the difference between $\varepsilon_{\rm M}$ and $\varepsilon_{\rm P}$ results in an unequal charge distribution at Au and C and leads to charge transfer between the metal and the molecule across the interface. Besides the on-site energy, the charge distribution depends on γ. In the right-handed helix/metal heterojunction, as shown by Fig. 1(a), the terminated metal atoms at the interface have different coupling strength with the molecule, which induces the nonuniform charge redistribution with chiral feature in the metal layers near the interface. Therefore, the chirality is transferred into the metal from the chiral molecule.

The chirality transfer due to the charge redistribution is then systemically studied. We define the metal layers with obvious chiral charge distribution as the interfacial region of the metal. It is found that about 8.55 electrons are transferred from the metal to the chiral molecule in the heterojunction where the number of metal sites is $N_{\rm M} = 40$ and the molecule length is $N_{\rm P} = 27$. The net charge redistribution near the interface is shown layer by layer in Fig. 2 where a two-dimensional Gaussian distribution centered on the lattice site is adopted as

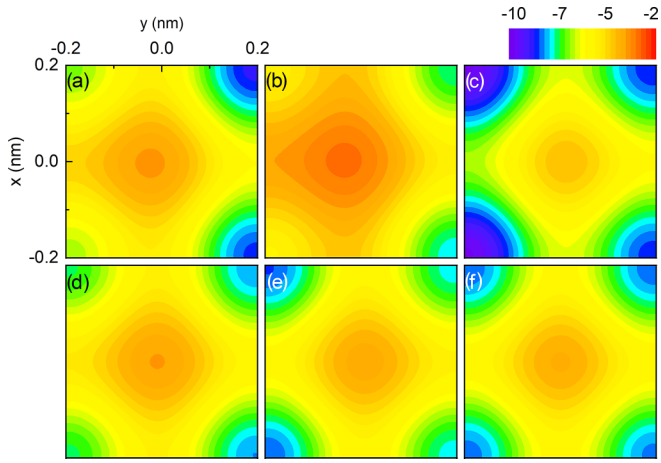

FIG. 2. Chiral charge density distribution in the metal corresponding to Fig. 1, numbered from (a) the first layer at interface to (f) the sixth layer away from the interface.

a continuum approach. The net charges on the four sites of the first layer are $-0.251e$, $-0.189e$, $-0.182e$, and $-0.242e$, where e is the electron charge. After the continuous treatment, the net charge distribution in this layer is shown in Fig. 2(a). Obviously, we could see that the charge distribution has no mirror symmetry for any plane perpendicular to the atomic layer, which indicates the chirality feature of distribution of charge density even though the lattice of the metal is achiral.

Further checking the charge distribution in the following layers, we find that the chirality is maintained within several layers of the metal and its strength decays slowly. As shown in Fig. 2, the charge density distribution near the interface shows strong chiral characteristics. By using the present parameters, we found that the chirality almost vanishes at the sixth layer and the pattern of the charge distribution returns to the symmetry of the lattice. Therefore, in a chiral molecule/metal heterojunction, in addition to the charge transfer, the chirality transfer occurs consequently. With the above calculations, we find that the chirality transfer is maintained in the interface within several layers of the metal. The chiral interface of the metal, together with the charge interface and spinterface, will determine the function of an electronic or spintronic device.

Due to the chirality transfer, as we discussed above, the interfacial region of the metal has the following characteristics: achiral simple orthogonal lattice structure, chiral charge distribution, and strong spin-orbit coupling. Especially, the chiral interface together with the strong spin-orbit coupling of the metal will generate interesting spin phenomena such as the well-known CISS effect. When an electron is injected into the molecule region from the metal substrate, at the chiral interface, the electron will move through a helical orbit with large angular momentum before entering the molecule. At the same time, the electron spin will be bound to this helical orbit through the spin-orbit coupling. In this way, we say that the spin orientation is determined by the molecular chirality, while the spin polarization intensity is determined by the spin-orbit coupling of the metal substrate. To validate our inference, we design a chiral device containing the heterojunction which is studied extensively in experiments and calculate the spin polarized transport. Both the chiral molecule and the interfacial region of the metal with chiral charge distribution are included in the scattering region as shown in Fig. 3(a). The two sides of the scattering region are connected to one-dimensional reservoirs of electrons respectively. The virtual leads are introduced to simulate the phase breaking and energy dissipation caused by inelastic scattering that is ubiquitous in materials.

The transmission of electrons from the pth lead with spin s' to the qth lead with spin s is written as

$$T_{qs,ps'} = \mathrm{tr}[\Gamma_{qs} G^r \Gamma_{ps'} G^a], \tag{5}$$

where $G^r = (G^a)^+$ is the retarded Green function, Γ_{ps} (p, q = B, T, d) describes the coupling between the scattering region and the pth lead. $\Gamma_{\mathrm{B/T}} = 1.0$ eV for the bottom/top lead and $\Gamma_{\mathrm{d}} = 0.01$ eV for virtual leads. Using the method described in Refs. [32,33], the transmission of electrons with spin s detected at the top electrode is then given by

$$T_{\mathrm{eff},s}(\varepsilon) = \sum_{s'} T_{\mathrm{T}s,\mathrm{B}s'} + \sum_{\mu\nu}\left[\left(\sum_{s'} T_{\mathrm{T}s,\mu s'}\right) W^{-1}_{\mu\nu}\left(\sum_{ss'} T_{\nu s,\mathrm{B}s'}\right)\right]. \tag{6}$$

For tunneling transport, when the electron is incident with an eigenenergy of ε_μ of the system, the transmission spectrum will demonstrate a resonant tunneling peak whose properties depend on the electron eigenwave function ψ_μ. The calculated transmission spectrum is shown in Figs. 3(b) and 3(c). The difference in transmission between spin-up and spin-down electrons indicates that the electronic transport process is spin selective. We define the spin polarization of transmitted electrons as $P = (T_{\mathrm{eff},\uparrow} - T_{\mathrm{eff},\downarrow})/(T_{\mathrm{eff},\uparrow} + T_{\mathrm{eff},\downarrow})$. As shown by the solid line in Fig. 3(d), with realistic parameters, a sizable spin polarization of about -15.4% is obtained. The spin polarization obtained in our calculation is comparable to that detected in the experiment of α-helical peptides [34]. The parameters we use here are prototypical, and the spin polarization can be further enhanced by elaborately adjusting the molecular geometry and other parameters. Performing the mirror symmetry operation on the right-handed helical molecule/metal heterojunction as shown in Fig. 3(a), the molecular chirality will be switched to left-handed. Therefore, the induced chirality in the interfacial region of the metal will be switched accordingly, which results in the reversal of the spin polarization which is reflected by the dashed curve in Fig. 3(d). We also notice that the spin selectivity of the heterojunction disappears when the helical molecule is stretched into a linear one, which is straightforward since the chiral configuration is eliminated.

In the CISS experiments, the interface coupling could be modulated by the deposition method and the SOC could be changed by using different metal as substrate. The dependence of spin polarization on the interface coupling is shown in Fig. 4(a). With the increase of coupling strength γ_0, the spin polarization of transmitted electrons is enhanced accordingly due to the increasing of the induced chirality in the metal, as we discussed above. Besides larger chirality, the stronger interface coupling indicates that the induced chiral charge

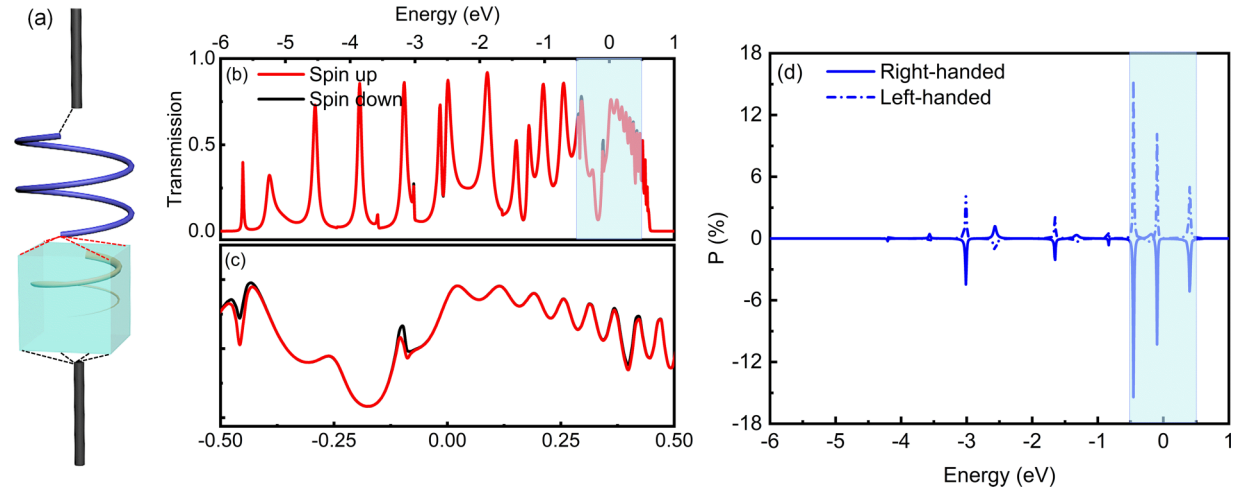

FIG. 3. (a) Schematic of the scattering region and the electrodes. The dashed line indicates the coupling at the interfaces. (b) Spin-related effective transmission spectrum of the modeled right-handed helix/metal heterojunction, where the area marked by blue shading is enlarged and plotted in (c), and (d) is the corresponding spin polarizations of two enantiomers.

distribution goes deeper into the metal. Therefore, the moving electrons in the metal transport in a longer path with the chiral spin-orbit coupling field, which contributes to the spin polarization. The effect of SOC strength α_0 on spin polarization is shown in Fig. 4(b). As α_0 increases, the intensities of most of main peaks increase. Since the SOC of the molecule is ignored in our model, it is interesting to find that the spin polarization is still sizable even when the SOC strength α_0 is weak. This result is consistent with the experimental studies that the substrate material does not have essential influence on the CISS effect [6].

In experiments, the spin polarization is measured with different lengths of helical molecules [7,35]. For example, in one experimental study of double-stranded DNA (dsDNA), the results of spin polarization as a function of the length of the molecule is shown by the red dots in Fig. 5 [7]. The length is measured in helical turns L. The result of our calculation is given by the solid line. Although the geometric structure parameters of the dsDNA molecule are not adopted to model the chiral molecule in the heterojunction, the following qualitative analyses and discussions will not be changed by the adjustment of molecular structural parameters. Disregarding the difference in magnitude due to the choice of parameters, we see that both the experimental data and theoretical results show similar trends, oscillating periodically with the molecule length. The oscillation comes from the quantum behavior of the moving electrons and the long-range transitions [17]. We can also see that the overall trend of spin polarization increases first and then decreases. Therefore, there is an optimal length of the chiral molecule for spin polarization. Our results match the previous study that the CISS effect is apparent only within a certain length of the chiral layer of several nanometers [36], and beyond this range of length, the spin

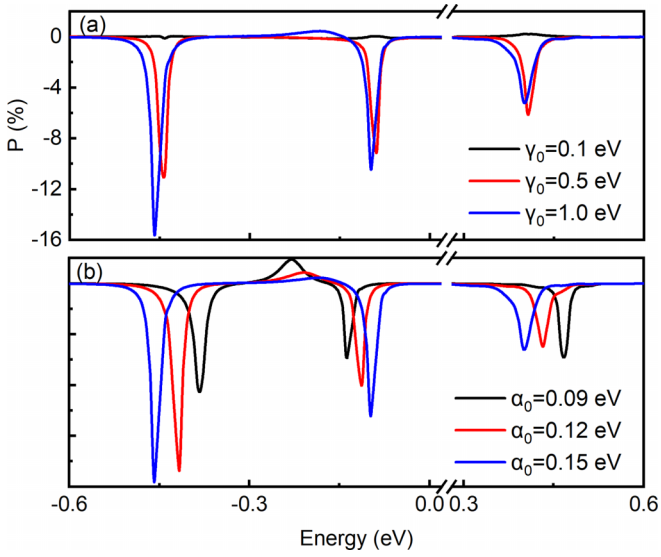

FIG. 4. Spin polarization of different (a) coupling strength γ_0 and (b) spin-orbit coupling strength α_0.

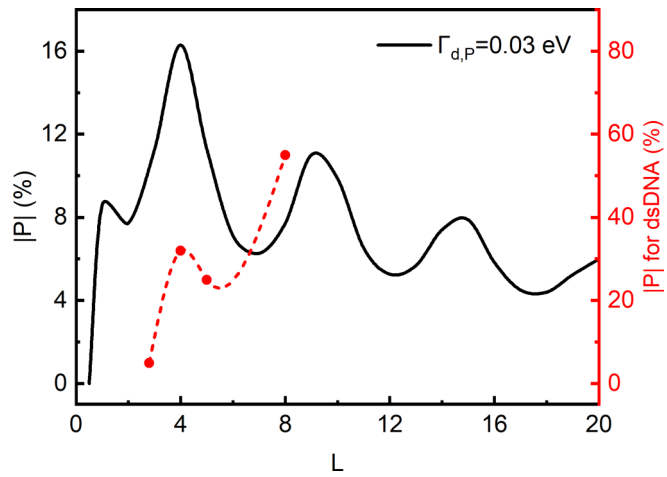

FIG. 5. Dependence of spin polarization on helical turns L. The black line is the calculated result. The red dots are the experimental data of spin polarization selected from Ref. [7]. The red dashed line is a guide to the eye.

polarization gradually decreases due to the influence of scattering.

III. CONCLUSIONS

In conclusion, we find the chirality transfer and the chiral interface in a molecule/metal heterojunction. It is predicated that the chiral interface will be a key factor for the performance of spin and orbit devices. The chiral feature of the achiral metal is induced by the chiral contact. The chirality of the charge distribution persists in several layers of the metal away from the interface, which provides an additional chiral channel for the moving electrons. Including the chiral interface and the strong spin-orbit coupling of the metal, with realistic parameters, we obtain a sizable spin selectivity effect. Our studies propose insights into the fundamental mechanisms of CISS and we hope to stimulate further studies on it.

ACKNOWLEDGMENTS

This work was supported by the National Natural Science Foundation of China (Grants No. 11974211 and No. 11974212) and the Major Program of the Natural Science Foundation of Shandong Province (Grant No. ZR2019ZD43). X.L. acknowledges the support from the Qilu Young Scholar Program of Shandong University.

The authors declare no competing financial interest.

[1] K. Ray, S. P. Ananthavel, D. H. Waldeck, and R. Naaman, Asymmetric scattering of polarized electrons by organized organic films of chiral molecules, Science **283**, 814 (1999).

[2] R. Naaman and D. H. Waldeck, Chiral-induced spin selectivity effect, J. Phys. Chem. Lett. **3**, 2178 (2012).

[3] R. Naaman and D. H. Waldeck, Spintronics and chirality: spin selectivity in electron transport through chiral molecules, Annu. Rev. Phys. Chem. **66**, 263 (2015).

[4] R. Naaman, Y. Paltiel, and D. H. Waldeck, Chiral molecules and the electron spin, Nat. Rev. Chem. **3**, 250 (2019).

[5] R. Naaman, Y. Paltiel, and D. H. Waldeck, Chiral molecules and the spin selectivity effect, J. Phys. Chem. Lett. **11**, 3660 (2020).

[6] M. Kettner, V. V. Maslyuk, D. Nürenberg, J. Seibel, R. Gutierrez, G. Cuniberti, K. Ernst, and H. Zacharias, Chirality-dependent electron spin filtering by molecular monolayers of helicenes, J. Phys. Chem. Lett. **9**, 2025 (2018).

[7] B. Göhler, V. Hamelbeck, T. Z. Markus, M. Kettner, G. F. Hanne, Z. Vager, R. Naaman, and H. Zacharias, Spin selectivity in electron transmission through self-assembled monolayers of double-stranded DNA, Science **331**, 894 (2011).

[8] A. K. Mondal, M. D. Preuss, M. L. Ślęczkowski, T. K. Das, G. Vantomme, E. W. Meijer, and R. Naaman, Spin filtering in supramolecular polymers assembled from achiral monomers mediated by chiral solvents, J. Am. Chem. Soc. **143**, 7189 (2021).

[9] V. Kiran, S. P. Mathew, S. R. Cohen, I. H. Delgado, J. Lacour, and R. Naaman, Helicenes—a new class of organic spin filter, Adv. Mater. **28**, 1957 (2016).

[10] O. B. Dor, S. Yochelis, S. P. Mathew, R. Naaman, and Y. Paltiel, A chiral-based magnetic memory device without a permanent magnet, Nat. Commun. **4**, 2256 (2013).

[11] G. Koplovitz, D. Primc, O. B. Dor, S. Yochelis, D. Rotem, D. Porath, and Y. Paltiel, Magnetic nanoplatelet-based spin memory device operating at ambient temperatures, Adv. Mater. **29**, 1606748 (2017).

[12] H. Al-Bustami, B. P. Bloom, A. Ziv, S. Goldring, S. Yochelis, R. Naaman, D. H. Waldeck, and Y. Paltiel, Optical multilevel spin bit device using chiral quantum dots, Nano Lett. **20**, 8675 (2020).

[13] Y. Kim, Y. Zhai, H. Lu, X. Pan, C. Xiao, E. A. Gaulding, S. P. Harvey, J. J. Berry, Z. V. Vardeny, J. M. Luther, and M. C. Beard, Chiral-induced spin selectivity enables a room-temperature spin light-emitting diode, Science **371**, 1129 (2021).

[14] M. Suda, Y. Thathong, V. Promarak, H. Kojima, M. Nakamura, T. Shiraogawa, M. Ehara, and H. M. Yamamoto, Light- driven molecular switch for reconfigurable spin filters, Nat. Commun. **10**, 2455 (2019).

[15] S. Yang, R. Naaman, Y. Paltiel, and S. S. P. Parkin, Chiral spintronics, Nat. Rev. Phys. **3**, 328 (2021).

[16] A. Guo and Q. Sun, Spin-selective Transport of Electrons in Dna Double Helix, Phys. Rev. Lett. **108**, 218102 (2012).

[17] A. Guo and Q. Sun, Spin-dependent electron transport in protein-like single-helical molecules, Proc. Natl. Acad. Sci. USA **111**, 11658 (2014).

[18] L. Zhang, Y. Hao, W. Qin, S. Xie, and F. Qu, Chiral-induced spin selectivity: A polaron transport model, Phys. Rev. B **102**, 214303 (2020).

[19] T. Gao, Q. Tian, M. Du, L. Zhang, X. Liu, W. Qin, and S. Xie, Synergistic effect of carrier velocity and density on chirality-induced spin selectivity in helical organic devices, Appl. Phys. Lett. **120**, 032405 (2022).

[20] J. Fransson, Vibrational origin of exchange splitting and chiral-induced spin selectivity, Phys. Rev. B **102**, 235416 (2020).

[21] J. Fransson, Chirality-induced spin selectivity: the role of electron correlations, J. Phys. Chem. Lett. **10**, 7126 (2019).

[22] D. Mishra, T. Z. Markus, R. Naaman, M. Kettner, B. Göhler, H. Zacharias, N. Friedman, M. Sheves, and C. Fontanesi, Spin-dependent electron transmission through bacteriorhodopsin embedded in purple membrane, Proc. Natl. Acad. Sci. USA **110**, 14872 (2013).

[23] L. Jia, C. Wang, Y. Zhang, L. Yang, and Y. Yan, Efficient spin selectivity in self-assembled superhelical conducting polymer microfibers, ACS Nano **14**, 6607 (2020).

[24] S. Mishra, A. K. Mondal, E. Z. B. Smolinsky, R. Naaman, K. Maeda, T. Nishimura, T. Taniguchi, T. Yoshida, K. Takayama, and E. Yashima, Spin filtering along chiral polymers, Angew. Chem. Int. Ed. **59**, 14671 (2020).

[25] Y. Liu, J. Xiao, J. Koo, and B. Yan, Chirality-driven topological electronic structure of DNA-like materials, Nat. Mater. **20**, 638 (2021).

[26] S. Alwan and Y. Dubi, Spinterface origin for the chirality-induced spin-selectivity effect, J. Am. Chem. Soc. **143**, 14235 (2021).

[27] J. Fransson, Charge redistribution and spin polarization driven by correlation induced electron exchange in chiral molecules, Nano Lett. **21**, 3026 (2021).

[28] T. Pan, A. Guo, and Q. Sun, Spin-polarized electron transport through helicene molecular junctions, Phys. Rev. B **94**, 235448 (2016).

[29] R. Gutierrez, E. Díaz, R. Naaman, and G. Cuniberti, Spin-selective transport through helical molecular systems, Phys. Rev. B **85**, 081404(R) (2012).

[30] G. Du, H. Fu, and R. Wu, Vibration-enhanced spin-selective transport of electrons in the DNA double helix, Phys. Rev. B **102**, 035431 (2020).

[31] S. Yeganeh, M. A. Ratner, E. Medina, and V. Mujica, Chiral electron transport: Scattering through helical potentials, J. Chem. Phys. **131**, 014707 (2009).

[32] X. Liu, X. Liu, and S. Xie, Chiral resistance effect in an organic helical heterojunction device, Appl. Phys. Lett. **121**, 113502 (2022).

[33] J. L. D'Amato and H. M. Pastawski, Conductance of a disordered linear chain including inelastic scattering events, Phys. Rev. B **41**, 7411 (1990).

[34] M. Kettner, B. Göhler, H. Zacharias, D. Mishra, V. Kiran, R. Naaman, C. Fontanesi, D. H. Waldeck, S. Sęk, J. Pawłowski, and J. Juhaniewicz, Spin filtering in electron transport through chiral oligopeptides, J. Phys. Chem. C **119**, 14542 (2015).

[35] H. Einati, D. Mishra, N. Friedman, M. Sheves, and R. Naaman, Light-controlled spin filtering in bacteriorhodopsin, Nano Lett. **15**, 1052 (2015).

[36] D. H. Waldeck, R. Naaman, and Y. Paltiel, The spin selectivity effect in chiral materials, APL Mater. **9**, 040902 (2021).